

Graph picture of linear quantum networks and entanglement

Seungbeom Chin*

*Department of Electrical and Computer Engineering,
Sungkyunkwan University, Suwon 16419, Korea*

Yong-Su Kim

*Center for Quantum Information, Korea Institute of Science and Technology (KIST), Seoul, 02792, Korea
Division of Nano & Information Technology, KIST School,
Korea University of Science and Technology, Seoul 02792, Korea*

Sangmin Lee†

College of Liberal Studies, Seoul National University, Seoul 08826, Korea

The indistinguishability of quantum particles is widely used as a resource for the generation of entanglement. Linear quantum networks (LQNs), in which identical particles linearly evolve to arrive at multimode detectors, exploit the indistinguishability to generate various multipartite entangled states by the proper control of transformation operators. However, it is challenging to devise a suitable LQN that carries a specific entangled state or compute the possible entangled state in a given LQN as the particle and mode number increase. This research presents a mapping process of arbitrary LQNs to graphs, which provides a powerful tool for analyzing and designing LQNs to generate multipartite entanglement. We also introduce the perfect matching diagram (PM diagram), which is a refined directed graph that includes all the essential information on the entanglement generation by an LQN. The PM diagram furnishes rigorous criteria for the entanglement of an LQN and solid guidelines for designing suitable LQNs for the genuine entanglement. Based on the structure of PM diagrams, we compose LQNs for fundamental N -partite genuinely entangled states.

I. INTRODUCTION

Entanglement is an essential property of multipartite quantum systems that works as a resource for several kinds of quantum information processing [1]. Among diverse methods to create entangled multipartite systems, the indistinguishability of quantum particles is frequently employed for obtaining such systems. As a well-known example, Hong-Ou-Mandel interference [2] showed that if two fully-indistinguishable photons are scattered so that their paths completely overlap, the two-photon state is entangled at two detectors (a $N00N$ state with $N = 2$). Based on a similar intuition that the path ambiguity of indistinguishable particles can generate entanglement, various protocols have been suggested for the entanglement of identical particles [3–6]. Recently, there have been quantitative studies on the relation among particle indistinguishability, spatial coherence, and bipartite entanglement [7–10]. In particular, the amount of entanglement is experimentally verified to be a monotonically increasing function of both indistinguishability and spatial coherence [10].

While the above works mainly focus on bipartite

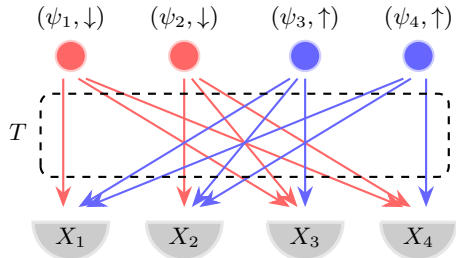
systems, another direction for exploiting the particle indistinguishability is the construction of general N -partite genuinely entangled states. Refs. [11, 12] suggested protocols for generating the N -partite W -state with spatially overlapped N identical particles and an ancilla. Ref. [13] designed linear multi-rail encoding networks for three photons to obtain tripartite GHZ and W states.

Despite the seemingly different forms of the physical setups, all the systems used in the aforementioned studies for the entanglement of identical particles can be conceptually considered *linear quantum networks* (LQN), in which each particle state is expressed as a local field that evolves linearly in space and time. An LQN consists of three elements (Fig. 1.a): N identical particles with d -dimensional internal degrees of freedom, a passive transformation operator T that transforms the initial particle states so that the final particle states are the linear combinations of the initial states, and M detectors that are distinctively located to each other. The N particles that evolve according to T are observed at M detectors. We can generate a variety of multipartite entangled states by controlling T . Indeed, the spatial overlap (or coherence) that is considered an essential factor for the entanglement in Refs. [7, 8, 10] is a special form of T .

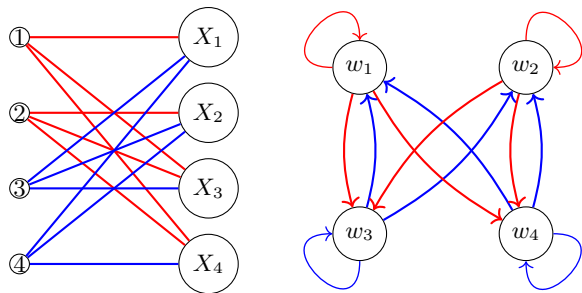
For an LQN, the ratio of N and M is a crucial factor for the non-classicality of quantum systems. For example, when $N \gg M$ with bosons, the sys-

* sbthesy@gmail.com

† sangmin@snu.ac.kr



(a) An $N = 4$ LQN. Each particle, initially at ψ_i (spatial wavefunction, $i = 1, 2, 3, 4$), evolves by the linear transformation operator T and arrives at the detectors X_i ($i = 1, 2, 3, 4$). The blue (red) color denotes the internal state \uparrow (\downarrow).



(b) The G_{bb} and G_d of the above LQN. From the structure of the graphs, we can directly read that the LQN carries a Dicke state. For a complete analysis of the entanglement in the graphs, see Section III B.

FIG. 1: A linear quantum network (LQN) with $N = M = 4$ and its corresponding graphs.

tem exhibits the Bose-Einstein condensation that can be simulated efficiently with a semiclassical approach [14]. On the other hand, when $N \ll M$, ideally indistinguishable bosons ($d = 1$) scattered by a linear unitary operator constitute the boson sampling setup [15]. Boson sampling is a very simple quantum implementation whose quantum advantage is experimentally verified [16].

In this work, we focus on another intriguing case where $N = M$ and each particle has two internal degrees of freedom, i.e., $d = 2$ (see Fig. 1.a for an $N = M = 4$ example). At the measurement level, we postselect the states for each detector to observe only one particle, i.e., *no particle-bunching states*. Then the state of each subsystem, which corresponds to a detector (spatial mode), is equivalent to the internal state of the particle that arrives at the detector. Thus the two internal states begin to play the role of qubits. Many schemes of LQNs for generating entanglement is based on this setup [5, 7, 11–13]. It was also shown that such a postselection is safe

from the selection bias [17].

A critical aspect of generating entanglement in this setup is the lack of any apparent relation between the structure of a LQN (particle paths and internal state distributions) and the entanglement in it. For this reason, the researches on the entanglement of LQN have remained in the case-by-case approach. Our main goal is to overcome the limitation with a graph picture.

In this research, we introduce a mapping process of such LQNs into graphs, which turns out to provide a powerful tool for analyzing the entanglement carried by the LQNs. The advantage of associating graph theory with quantum information processing has been validated in many works: quantum graph states [18–21], the linkage of undirected graphs to optical setups involving multiple crystals [22–25], and Gaussian boson sampling exploited to solve the computational complexity problems in graph theory [26–28]. Here, we show that *the graph picture of LQNs is also beneficial for computing the entanglement of no-bunching states in LQNs*. Moreover, by showing that the graph structure is closely related to the entanglement property of the corresponding LQNs, *we can reversely propose a protocol for designing optimal LQNs that generate specific N -partite entangled states*.

The result of this work is divided into two parts: The first part explains how LQNs of our interest can be mapped into graphs, and exploits graph-theoretical techniques for computing the entanglement of LQNs. We achieve a graph picture of an LQN by inserting all the indispensable quantities in the LQN into the weighted and colored adjacency matrices A and C , which combine to draw graphs of colored weighted edges. By slightly varying the mapping relations, an LQN can be represented as two types of graphs, a *balanced bipartite graph* G_{bb} and a *directed graph* G_d (the mathematical definitions of the graph theory are summarized in Appendix A). Fig. 1.b presents the graph picture of an $N = 4$ example. We show how the combined use of the two representations provides a convenient protocol to compute the final no-bunching state that we postselect.

The second part introduces the concept of *perfect matching (PM) diagram* \overline{G}_d , which is a refined G_d -representation of LQNs that includes the essential information of LQNs. A \overline{G}_d corresponds to an LQN that only contains the particle paths that contribute to the postselected no-bunching states. Hence, we can analyze the entanglement property of an LQN by examining the \overline{G}_d structure. Moreover, the \overline{G}_d -representation provides strong guidelines to build LQNs that carry specifically entangled no-bunching

states. Indeed, we suggest LQNs that generates the N -partite GHZ class, W class, and Dicke states designed from the \overline{G}_d structure.

Therefore, we can state that *the graph picture of LQNs enables a schematic approach to the two central procedures for the entanglement of LQNs*, i.e., designing an appropriately entangled LQN and extracting no-bunching states in the LQN.

II. COMPUTING LQN STATES WITH GRAPHS

Here, we provide the mathematical formulation of LQNs and then explain how an LQN is mapped to two forms of graphs, G_{bb} and G_d . We are interested in the postselection of no-bunching states and the evaluation of the entanglement carried by the states. Thus, an essential part of quantifying the entanglement is to compute the no-bunching states. Using the fact that such states correspond to *perfect matchings* (PMs, see Appendix A) in the G_{bb} -representation, we propose a simple and intuitive protocol for obtaining the total no-bunching state in an LQN.

A. Linear quantum network (LQN)

A quantum network of N particles, which evolve in spacetime and arrive at M spatially distinctive detectors, is *linear* if the initial state of each particle is linearly related to the final detector states, and vice versa. As we have mentioned in the introduction, we study the LQNs of $N = M$ and two-dimensional internal state ($d = 2$) with the computational basis $\{\uparrow, \downarrow\}$.

We denote the initial state of an a th particle as $\Psi_a = (\psi_a, s_a)$ (ψ_a : the particle spatial wavefunction, s_a : the internal state, and $a = 1, \dots, N$), and the detector spatial wavefunctions as ϕ_j ($j = 1, \dots, N$). The wavefunctions are set to be orthonormal without loss of generality. Then, the linear evolution of a particle in Ψ_a to the j th detector is expressed as

$$|\Psi_a\rangle = |\psi_a, s_a\rangle = \sum_{j=1}^N T_{aj} |\phi_j, r_j^a\rangle, \quad (T_{aj} \in \mathbb{C}) \quad (1)$$

where the transformation amplitude T_{aj} is normalized as $\sum_j |T_{aj}|^2 = 1$ so that the particle states evolve probabilistically, and r_j^a is the internal state of a particle that leaves ψ_a for ϕ_j . The above equation is equivalently expressed with the field operators of

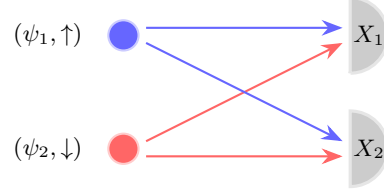


FIG. 2: An $N = 2$ LQN example. Two identical particles with opposite internal states can generate an entangled no-bunching state by the spatial PM with two detectors.

the second quantization language as

$$\hat{a}_{as_a}^\dagger = \sum_{j=1}^N T_{aj} \hat{b}_{jr_j^a}^\dagger, \quad (2)$$

where $\hat{a}_{as_a}^\dagger |vac\rangle \equiv |\psi_a, s_a\rangle$ and $\hat{b}_{jr_j^a}^\dagger |vac\rangle \equiv |\phi_j, r_j^a\rangle$.

Then the total N -particle state transformation is given by

$$\prod_{a=1}^N \hat{a}_{as_a}^\dagger |vac\rangle = \prod_{a=1}^N \left(\sum_{j=1}^N T_{aj} \hat{b}_{jr_j^a}^\dagger \right) |vac\rangle. \quad (3)$$

At the detector level, we postselect only the *no-bunching states*, i.e., the cases when each detector observes only one particle. Then the superposition of such states determine the entanglement observed at the output detectors.

As a simple example, suppose that two bosons at two separated places with different internal states ($\hat{a}_{1\uparrow}^\dagger$ and $\hat{a}_{2\downarrow}^\dagger$, see Fig. 2) transform to

$$\begin{aligned} \hat{a}_{1\uparrow}^\dagger &= \alpha_1 \hat{b}_{1\uparrow}^\dagger + \beta_1 \hat{b}_{2\uparrow}^\dagger, \\ \hat{a}_{2\downarrow}^\dagger &= \alpha_2 \hat{b}_{1\downarrow}^\dagger + \beta_2 \hat{b}_{2\downarrow}^\dagger. \end{aligned} \quad (4)$$

with $|\alpha_1|^2 + |\beta_1|^2 = |\alpha_2|^2 + |\beta_2|^2 = 1$. In the form of Eq. (3), we set

$$\begin{aligned} (T_{11}, T_{12}, T_{21}, T_{22}) &= (\alpha_1, \beta_1, \alpha_2, \beta_2), \\ (r_1^1, r_2^1, r_1^2, r_2^2) &= (\uparrow, \uparrow, \downarrow, \downarrow). \end{aligned} \quad (5)$$

Then the state transformation is given by

$$\begin{aligned} \hat{a}_{1\uparrow}^\dagger \hat{a}_{2\downarrow}^\dagger |vac\rangle &= (\alpha_1 \hat{b}_{1\uparrow}^\dagger + \beta_1 \hat{b}_{2\uparrow}^\dagger) (\alpha_2 \hat{b}_{1\downarrow}^\dagger + \beta_2 \hat{b}_{2\downarrow}^\dagger) |vac\rangle \\ &= (\alpha_1 \alpha_2 \hat{b}_{1\uparrow}^\dagger \hat{b}_{1\downarrow}^\dagger + \alpha_1 \beta_2 \hat{b}_{1\uparrow}^\dagger \hat{b}_{2\downarrow}^\dagger \\ &\quad + \beta_1 \alpha_2 \hat{b}_{2\uparrow}^\dagger \hat{b}_{1\downarrow}^\dagger + \beta_1 \beta_2 \hat{b}_{2\uparrow}^\dagger \hat{b}_{2\downarrow}^\dagger) |vac\rangle. \end{aligned} \quad (6)$$

By postselecting no-bunching states, the (unnormalized) final state to be measured is given by

$$\begin{aligned} |\Psi_{\text{fin}}\rangle &= (\alpha_1 \beta_2 \hat{b}_{1\uparrow}^\dagger \hat{b}_{2\downarrow}^\dagger + \beta_1 \alpha_2 \hat{b}_{2\uparrow}^\dagger \hat{b}_{1\downarrow}^\dagger) |vac\rangle \\ &\equiv \alpha_1 \beta_2 |\uparrow_1, \downarrow_2\rangle \pm \beta_1 \alpha_2 |\downarrow_1, \uparrow_2\rangle. \end{aligned} \quad (7)$$

where $+$ for bosons and $-$ for fermions in the last line. This is an entangled state of mode X_1 and X_2 with concurrence $E_c(|\Psi_{\text{fin}}\rangle) = 4|\alpha_1\alpha_2\beta_1\beta_2|$ [7, 8, 10]. Note that $E_c = 0$ when either of the particles arrives at one detector with probability 1 (no spatial coherence).

B. Graph picture of LQN

While the above $N = 2$ example is relatively easy to treat, it becomes quickly complicated as N increases to evaluate the entanglement carried by no-bunching states in an LQN. On the other hand, we can map LQNs into graphs, in which the computation usually becomes much easier. Here, we formalize the mapping of LQNs into graphs.

The graph picture of an LQN can be achieved by inserting all the indispensable variables of LQN in Eq. (3) into the weighted adjacency matrix A and the colored adjacency matrix C , which combine to draw a graph with colored weighted edges. Eq. (3) denotes that a particle in (ψ_a, s_a) arrives at the j th detector with probability $|T_{aj}|^2$ and internal state r_j^a , which is set to be \uparrow or \downarrow [29]. Note that s_a becomes irrelevant to the final state since it is replaced by r_j^a in the transformation process. Thus, T_{aj} and r_j^a are the quantities that we must keep through the mapping.

As a result, if we insert T_{aj} into the elements of A and r_j^a into those of C as

$$A_{aj} = T_{aj} \quad (\in \mathbb{C}), \quad C_{aj} = r_j^a \quad (\in \mathbb{Z}_2), \quad (8)$$

the graph determined by A and C fully contains the relevant information on the LQN. Note that A and C always have the same number of non-zero entries.

Considering the relation of adjacency matrices with graphs (see Appendix A), the mapping relations Eq. (8) imply that the particle index a and the detector index j in LQN become the vertex indices, and the internal state r_j^a becomes the color of an edge connecting vertices a and j in the graph picture. We set the edge color blue (B) for $r_j^a = \uparrow$ and red (R) for $r_j^a = \downarrow$.

In graph theory, it is well-known that an $(N \times N)$ -adjacency matrix can construct two types of graphs, i.e., a *directed graph* G_d and an *undirected balanced bigraph* G_{bb} , according to how we define the relation of indices a and j with vertices (see, e.g., Ref. [30]).

First, we can consider both a and j as the indices of a N -vertex set $W = \{w_1, w_2, \dots, w_N\}$. Then, A_{aj} (C_{aj}) indicate the weight (color) of an edge from w_a to w_j . Such $(N \times N)$ -matrices, denoted as A_d and C_d , become the adjacency matrices of a directed

graph $G_d = (W, F)$. In this G_d -representation, one particle and one detector are mapped to the same vertex in W .

On the other hand, we can also consider a and j as indices of two different vertex sets, i.e., a as the index of a vertex set $U = \{u_1, u_2, \dots, u_N\}$ and j as that of another set $V = \{v_1, v_2, \dots, v_N\}$. Then a balanced bigraph $G_{bb} = (U \cup V, E)$ is constructed by setting the adjacency matrices A_{bb} and C_{bb} as symmetric forms

$$A_{bb} = \begin{pmatrix} 0 & A_d \\ (A_d)^T & 0 \end{pmatrix}, \quad C_{bb} = \begin{pmatrix} 0 & C_d \\ (C_d)^T & 0 \end{pmatrix}, \quad (9)$$

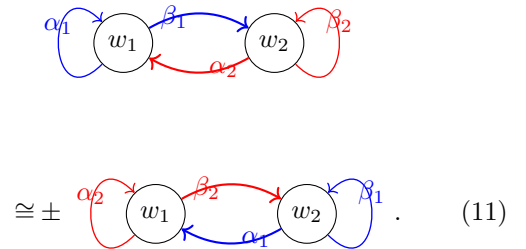
where $(A_d)^T$ and $(C_d)^T$ are the transposes of A_d and C_d . From the fact that particles and detectors are mapped distinctively, the G_{bb} -representation depicts an LQN in a very intuitive manner. However, the G_d -representation is also advantageous for analysing some crucial hidden structures of the LQN, which we will discuss in Section IID.

An important feature of A_d and C_d from an LQN is that they are *symmetric (antisymmetric) under the exchange of rows according to the exchange symmetry (antisymmetry) of bosons (fermions) in the LQN*. Therefore, if two G_{bb} become identical by any exchange of vertices in U , we consider them an equivalent graph that corresponds to the same LQN.

To elucidate the mapping process of an LQN into graphs, we see how the $N = 2$ example in Fig. 2 is mapped to graphs. By substituting Eq. (5) into Eq. (8), A_d and C_d in the G_d -representation are given by

$$\begin{aligned} A_d &= \begin{pmatrix} \alpha_1 & \beta_1 \\ \alpha_2 & \beta_2 \end{pmatrix} \cong \pm \begin{pmatrix} \alpha_2 & \beta_2 \\ \alpha_1 & \beta_1 \end{pmatrix}, \\ C_d &= \begin{pmatrix} B & B \\ R & R \end{pmatrix} \cong \pm \begin{pmatrix} R & R \\ B & B \end{pmatrix} \\ & \text{(+ for bosons and - for fermions)} \end{aligned} \quad (10)$$

(\cong means two adjacency matrices are physically identical by the exchange symmetry), which draws a G_d ,



Linear quantum network (LQN)	Balanced bigraph $G_{bb} = (U \cup V, E)$
N identical particles	N identical vertices $\in U$
N detectors	N non-identical vertices $\in V$
Possible paths of particles to arrive at detectors	Edges $\in E$
Probability amplitudes	Edge weights ($\in \mathbb{C} \setminus 0$)
Internal states (\uparrow and \downarrow)	Edge colors (B and R)
No-bunching states	Perfect matchings (PMs)

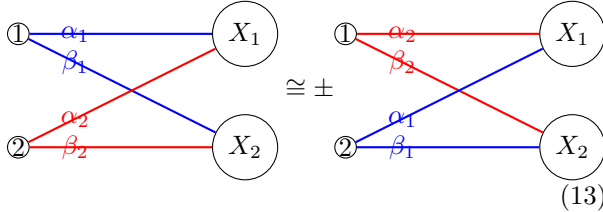
TABLE I: The correspondence relations between the elements of LQN and G_{bb}

For the same $N = 2$ LQN, A_{bb} and C_{bb} in the G_{bb} -representation are given by

$$A_{bb} = \begin{pmatrix} 0 & 0 & \alpha_1 & \beta_1 \\ 0 & 0 & \alpha_2 & \beta_2 \\ \alpha_1 & \alpha_2 & 0 & 0 \\ \beta_1 & \beta_2 & 0 & 0 \end{pmatrix} \cong \pm \begin{pmatrix} 0 & 0 & \alpha_2 & \beta_2 \\ 0 & 0 & \alpha_1 & \beta_1 \\ \alpha_2 & \alpha_1 & 0 & 0 \\ \beta_2 & \beta_1 & 0 & 0 \end{pmatrix},$$

$$C_{bb} = \begin{pmatrix} 0 & 0 & B & B \\ 0 & 0 & R & R \\ B & R & 0 & 0 \\ B & R & 0 & 0 \end{pmatrix} \cong \pm \begin{pmatrix} 0 & 0 & R & R \\ 0 & 0 & B & B \\ R & B & 0 & 0 \\ R & B & 0 & 0 \end{pmatrix}, \quad (12)$$

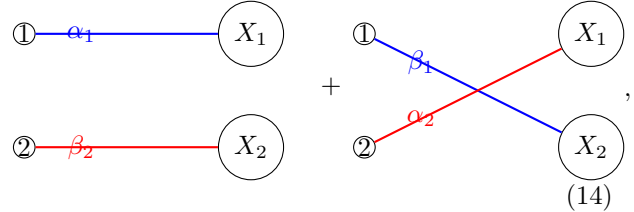
which draws a G_{bb} ,



In the above G_{bb} , we used a ($= 1, 2, \dots, N$) for the vertex index of U and X_j ($j = 1, 2, \dots, N$) for that of V , which will be the standard notation

from now on. By comparing Eq. (13) with Fig. 2, we see that the G_{bb} -representation straightforwardly describes the LQN structure. Two vertices with indices 1 and 2 denote two identical particles. The edges correspond to the particle paths to detectors, the edge weights ($\in \mathbb{C} \setminus 0$) to the probability amplitudes, the edge colors ($\in \mathbb{Z}_2$) to the internal states of the particles along the paths.

The postselection of no-bunching states at the detectors correspond to the collection of N edges that connect completely different vertices in the G_{bb} -representation. Such edge sets are called *perfect matchings* (PMs) in graph theory (Appendix A). The case of (13) carries two perfect matchings,



which correspond to the two terms of Eq. (7).

The correspondence relations between LQN and G_{bb} are summarized in Table I.

C. Computing the no-bunching states in G_{bb} -representation

By generalizing the procedure from Eq. (13) to Eq. (14), we can construct a systematic computation protocol for directly extracting the no-bunching states of a given LQN in the G_{bb} -representation:

Computation protocol

1. Using the mapping relation (9), write down the adjacency matrices A_{bb} and C_{bb} of the G_{bb} -representation.

2. Draw the corresponding G_{bb} .

3. Find all the PMs in the G_{bb} .

4. Write down the no-bunching states corresponding to the PMs. For a no-bunching state, the internal state of the j th detector is determined by the color of the edge attached to X_j in the PM. The amplitude for the state is obtained by multiplying all the weights of the edges in the PM.

Note that Step 1 can be skipped when the pictorial relation between the LQN and G_{bb} is clear.

By obtaining the relevant no-bunching terms directly from PMs in the G_{bb} , the computation of the final postselected states become much simpler with the protocol.

As an example, we compute a bosonic $N = 3$ LQN whose transformation is given by a tritter (Figure 3), which performs a balanced unitary transformation of three boson states with no internal state rotation. With two bosons initially in \uparrow and one boson in \downarrow , the total state transformation relation with a tritter is written as

$$\begin{aligned} & \hat{a}_{1\uparrow}\hat{a}_{2\uparrow}\hat{a}_{3\downarrow}|vac\rangle \\ &= (u_{11}\hat{a}_{1\uparrow} + u_{12}\hat{a}_{2\uparrow} + u_{13}\hat{a}_{3\uparrow}) \\ & \times (u_{21}\hat{a}_{1\uparrow} + u_{22}\hat{a}_{2\uparrow} + u_{23}\hat{a}_{3\uparrow}) \\ & \times (u_{31}\hat{a}_{1\downarrow} + u_{32}\hat{a}_{2\downarrow} + u_{33}\hat{a}_{3\downarrow})|vac\rangle, \end{aligned} \quad (15)$$

with the unitary transformation matrix

$$U_3 = \begin{pmatrix} u_{11} & u_{12} & u_{13} \\ u_{21} & u_{22} & u_{23} \\ u_{31} & u_{32} & u_{33} \end{pmatrix} = \frac{1}{\sqrt{3}} \begin{pmatrix} 1 & \omega & \omega^2 \\ \omega & 1 & \omega^2 \\ 1 & 1 & 1 \end{pmatrix}, \quad (16)$$

where $\omega = e^{i\frac{2\pi}{3}}$.

The expansion of Eq. (15) contains $3^3 = 27$ terms. However, we can directly enumerate all the relevant no-bunching terms with our computation protocol as follows:

Steps 1 and 2. We can directly draw the corresponding G_{bb} of Fig. 3 as

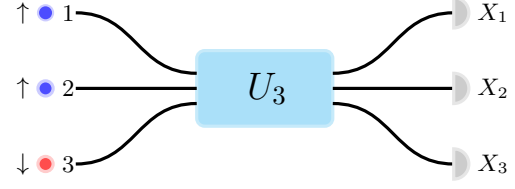
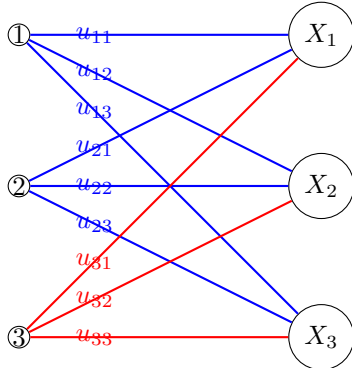
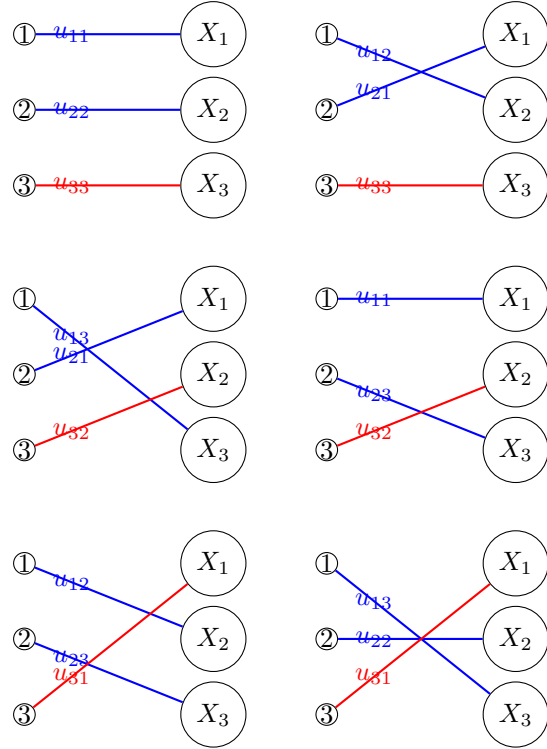


FIG. 3: An $N = 3$ LQN with a tritter. Two bosons with \uparrow are injected to input modes 1 and 2, and a boson with \downarrow is injected to 3. The total transformation matrix U_3 is unitary as Eq. (16), and we postselect no-bunching states (one particle per output detector X_j , $j = 1, 2, 3$).

Step 3. The above G_b has six PMs, which are



Step 4. By the exchange symmetry, the two PMs in the same line gives the same no-bunching terms. Therefore, the unnormalized final state at the level of detectors is given by

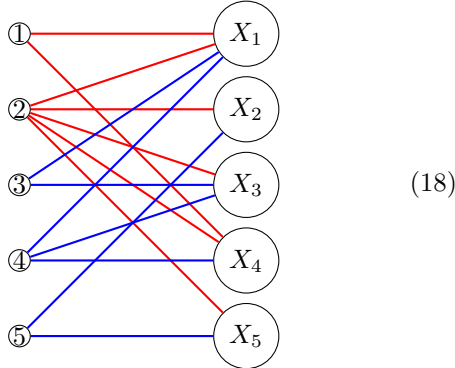
$$\begin{aligned} |\Psi_{fin}\rangle &= (u_{11}u_{22} + u_{12}u_{21})u_{33}|\uparrow_1\uparrow_2\downarrow_3\rangle \\ &+ (u_{13}u_{21} + u_{11}u_{23})u_{32}|\uparrow_1\downarrow_2\uparrow_3\rangle \\ &+ (u_{12}u_{23} + u_{13}u_{22})u_{31}|\downarrow_1\uparrow_2\uparrow_3\rangle \\ &\sim |\uparrow_1\uparrow_2\downarrow_3\rangle + \omega|\uparrow_1\downarrow_2\uparrow_3\rangle + \omega^2|\downarrow_1\uparrow_2\uparrow_3\rangle. \end{aligned} \quad (17)$$

Finally, we have obtained a tripartite W state by extracting the relevant six terms, not dealing with the whole $3^3 = 27$ terms that the LQN contains.

From now on, we suppose the particles are bosons for simplicity. A fermionic extension for the same LQN is easily achieved by applying the particle exchange *anti*-symmetry instead of the symmetry.

D. Finding PMs in the G_d -representation

When our computation protocol is applied to an arbitrary N particle LQN, the most non-trivial part is to enumerate all the PMs in the given G_{bb} . Although it was not very complicated for $N = 2$ and $N = 3$ examples we have discussed, we need a well-established protocol to find PMs in an LQN as the particle and edge numbers increase. For example, see the following $N = 5$ bipartite graph

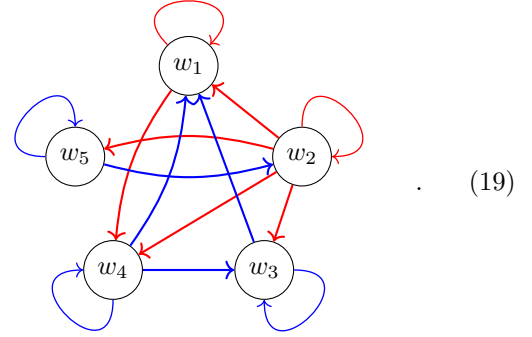


(whenever the edge weights are omitted in graphs, we presume they are set to be arbitrary T_{aj} for (a, X_j)). It can be implemented in the optical setup with the second particle sent through 5×5 multiport, the fourth through a 3×3 multiport, and the others through beam splitters.

Here, we explain a systematic method to find PMs by mapping the G_{bb} to a G_d and examining the topology of the G_d . It was shown in Refs. [31, 32] that for a G_{bb} with non-zero PMs, the existence of a PM is equivalent to that of an elementary cycle (a circular path that does not pass the same vertex twice, see Appendix A) in the G_d . We can use the relation to find all the no-bunching states of an LQN.

We can draw a G_d directly from a $G_b = (U \cup V, E)$ by mapping two vertices $i \in U$ and $X_i \in V$ to one vertex $w_i \in W$, and a undirected edge $(i, X_j) \in E$ to a directed edge $(w_i \rightarrow w_j) \in F$. For the

case of (18), the G_d is given by



We can consider a protocol to find PMs in a G_{bb} by looking into elementary cycles in the G_d :

PM-finding protocol

1. If there is more than one PM, we can label the vertices such that each vertex in G_d has a loop without loss of generality. Then the N loops constitute a PM, $\{(1, X_1), (2, X_2), \dots, (N, X_N)\}$.

2. If there is an elementary cycle

$$(w_{i_1} \rightarrow w_{i_2} \rightarrow \dots \rightarrow w_{i_k} \rightarrow w_{i_1})$$

in the G_d , then the edge set

$$\underbrace{\{(i_1, X_{i_2}), (i_2, X_{i_3}), \dots, (i_{k-1}, X_{i_k}), (i_k, X_{i_1}), (i_{k+1}, X_{i_{k+1}}), \dots, (i_N, X_{i_N})\}}_{\text{edge exchange along the elementary cycle}}$$

$(1 \leq i_q \leq N$ for $1 \leq q \leq N$, and $i_q = i_p$ if and only if $q = p$) is also a PM in G_b .

3. Repeat Step 2 until we exhaust all the elementary cycles in the G_d . Note that if there are elementary cycles that have no overlapping vertex with each other, a simultaneous edge exchange of such cycles also results in a PM.

Applying the above protocol to (19), we first see that the five loops attached to the vertices in (19) gives a PM,

$$\{(1, X_1), (2, X_2), (3, X_3), (4, X_4), (5, X_5)\}. \quad (20)$$

There are three elementary cycles,

$$\begin{aligned} &(w_2 \rightarrow w_5 \rightarrow w_2), \\ &(w_1 \rightarrow w_4 \rightarrow w_1), \\ &(w_1 \rightarrow w_4 \rightarrow w_3 \rightarrow w_1), \end{aligned} \quad (21)$$

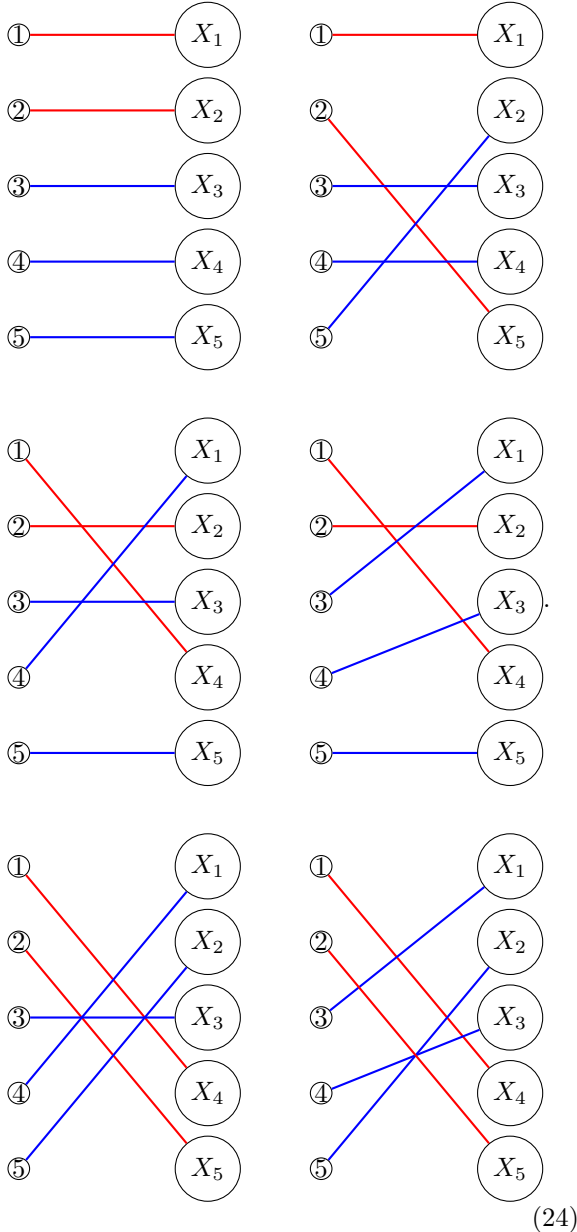
which give three PMs,

$$\begin{aligned} & \{(2, X_5), (5, X_2), (1, X_1), (3, X_3), (4, X_4)\}, \\ & \{(1, X_4), (4, X_1), (2, X_2), (3, X_3), (5, X_5)\}, \\ & \{(1, X_4), (4, X_3), (3, X_1), (2, X_2), (5, X_5)\}. \end{aligned} \quad (22)$$

Note that $(w_2 \rightarrow w_5 \rightarrow w_2)$ and $(w_1 \rightarrow w_4 \rightarrow w_1)$ do not share any vertex, and neither do $(w_2 \rightarrow w_5 \rightarrow w_2)$ and $(w_1 \rightarrow w_4 \rightarrow w_3 \rightarrow w_1)$. Therefore, simultaneous edge exchanges of them give two more PMs,

$$\begin{aligned} & \{(1, X_4), (4, X_1), (2, X_5), (5, X_2), (3, X_3)\}, \\ & \{(2, X_5), (5, X_2), (1, X_4), (4, X_3), (3, X_1)\}. \end{aligned} \quad (23)$$

In total, (19) gives 6 PMs, which are drawn in the G_{bb} -representation as



Mapping the PMs into the no-bunching states in the LQN, the unnormalized form of the final no-bunching state is written as

$$\begin{aligned} & |\Psi_{fin}\rangle \\ & = T_{11}T_{22}T_{33}T_{44}T_{55}|\downarrow_1\downarrow_2\uparrow_3\uparrow_4\uparrow_5\rangle \\ & + T_{11}T_{52}T_{33}T_{44}T_{25}|\downarrow_1\uparrow_2\uparrow_3\uparrow_4\downarrow_5\rangle \\ & + (T_{41}T_{22}T_{33} + T_{31}T_{22}T_{43})T_{14}T_{55}|\uparrow_1\downarrow_2\uparrow_3\downarrow_4\uparrow_5\rangle \\ & + (T_{41}T_{52}T_{33} + T_{31}T_{52}T_{43})T_{14}T_{25}|\uparrow_1\uparrow_2\uparrow_3\downarrow_4\downarrow_5\rangle. \end{aligned} \quad (25)$$

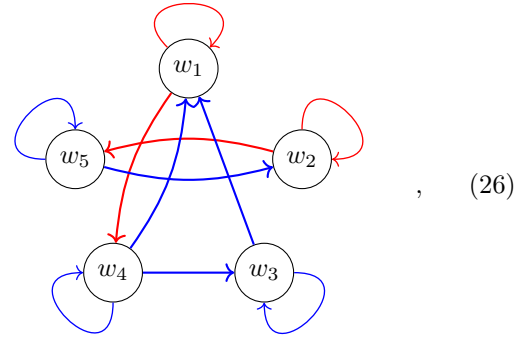
As we have shown, we can schematically compute the postselected no-bunching state for any form of LQNs by combining the computation protocol in G_{bb} and the above PM-finding protocol in G_d .

III. PERFECT MATCHING DIAGRAM AND THE ENTANGLEMENT OF LINEAR QUANTUM NETWORKS

A crucial observation in the process of enumerating PMs is that not all the edges in G_d are relevant for constituting the final no-bunching state. Considering the $N = 5$ example (18) again, we can see that the edges $(2, X_1)$, $(2, X_4)$, and $(2, X_5)$ are not included in any PM from the fact that they are not in any elementary cycle in (19). With this in consideration, we define a subgraph of the G_d for a streamlined analysis of the entanglement generation by an LQN:

Definition 1. (*perfect matching diagram*) For a given G_d , we define a “perfect matching diagram” (PM diagram, \overline{G}_d) of the G_d as a directed subgraph in which only the loops and the edges included the elementary cycles of the G_d are retained.

Then all the edges in a \overline{G}_d are included in the PMs of the LQN. Since a \overline{G}_d has no dummy particle path that are irrelevant to the no-bunching states, it captures the physical essence of the LQN. For example, the \overline{G}_d of (19) is drawn as



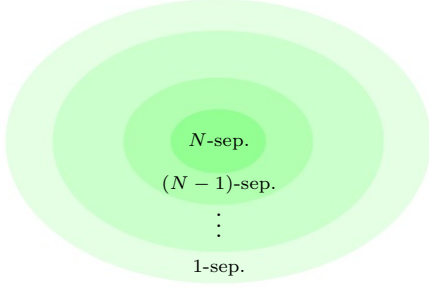


FIG. 4: The inclusion relation of k -separable states. If a state is k -separable, then it is trivially $k-1$ -separable. The states in the innermost circle is N -separable/entangled, i.e., *fully separable*, and those in the outermost ring is 1-separable/entangled, i.e., *genuinely entangled*.

which gives the same perfect matchings as (19). Finding the \overline{G}_d of an LQN is equivalent to finding maximally-matchable edges (edges in at least one of the PMs, see Appendix A) of a G_{bb} , which is efficiently achieved in $\mathcal{O}(N+L)$ steps [32].

Reversely, when we build an LQN to obtain some entangled no-bunching state, we should make its G_d to be equal to \overline{G}_d , i.e., all vertices in elementary cycles, to avoid dummy paths from the beginning.

In this section, we will present some rigorous relations between the structure of a \overline{G}_d and the entanglement of the total no-bunching state in the LQN. We show that for an LQN to generate a N -partite genuinely entangled state, the \overline{G}_d must be strongly connected and each vertex in it must have more than two incoming edges of different colors. We employ this relation to design LQNs fundamental genuinely entangled states.

A. \overline{G}_d structure and the entanglement of LQNs

Before scrutinizing the relation between the structure of \overline{G}_d and entanglement, we summarize the criteria for discriminating the hierarchy of pure state entanglement in multipartite systems. For a more thorough explanation including mixed states, see, e.g., Refs. [33, 34].

For a general N -partite system, the degree of entanglement for a pure state is widely categorized into three classes. First, a pure state $|\psi\rangle$ ($\in \mathcal{H} = \otimes_{j=1}^N \mathcal{H}_j$) is *fully separable* if it can be written as $|\psi\rangle = |\psi_1\rangle \otimes |\psi_2\rangle \otimes \cdots \otimes |\psi_N\rangle$ where $|\psi_j\rangle \in \mathcal{H}_j$ for all $j = 1, 2, \dots, N$. Second, the state is *genuinely (fully) entangled* if $|\psi\rangle \neq |\phi\rangle_S \otimes |\chi\rangle_{\bar{S}}$ for any bipartition $S|\bar{S}$ ($S \cup \bar{S} = \mathcal{H}$ and $S \cap \bar{S} = \emptyset$). Third, the

state is *partially separable* when it is not fully separable but there exists at least one bipartition $S|\bar{S}$ of \mathcal{H} such that $|\psi\rangle = |\phi\rangle_S \otimes |\chi\rangle_{\bar{S}}$.

The partially separable states are divided into many classes according to the possible number of partitions. More specifically, a state is k -separable ($1 \leq k \leq N$) if there exists a k -partition $\alpha_k = S_1|S_2|\cdots|S_k$ of \mathcal{H} ($S_1 \cup S_2 \cup \cdots \cup S_k = \mathcal{H}$ and $S_a \cap S_b = \emptyset$ for any a and b between 1 and k) such that $|\psi\rangle$ is written as $|\psi\rangle = |\psi_{S_1}\rangle \otimes |\psi_{S_2}\rangle \otimes \cdots \otimes |\psi_{S_k}\rangle$ with $|\psi_{S_a}\rangle \in S_a$ for $a = 1, \dots, k$. It is trivial to see that a k -separable state is always $(k-1)$ -separable. If a state is k -separable but not $(k+1)$ -separable, it is called *k-separable/entangled*. 1-separable/entangled states are genuinely entangled, and N -separable/entangled states are fully separable. Fig. 4 shows the inclusion relation of the k -separability hierarchy.

We can show how the structure of a \overline{G}_d reveals the separability conditions of the no-bunching state in the LQN. First, one of the most obvious relations between the structure of \overline{G}_d and the entanglement of an LQN can be stated as the following lemma.

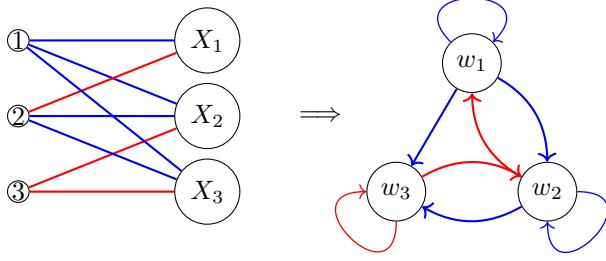
Lemma 1. *A subsystem X_i of an LQN is separable from the other subsystems in the computational basis ($|\uparrow\rangle$ or $|\downarrow\rangle$) if and only if all incoming edges of the corresponding vertex w_i in the \overline{G}_d are of the same color (a special case is when w_i has only one incoming edge from a loop).*

Proof. First, suppose that the incoming edges of w_i have the same color. Then, according to the PM-finding protocol, the subsystem X_i can have only one state ($|\uparrow\rangle$ or $|\downarrow\rangle$) in any PM. Conversely, suppose that a final total no-bunching state is written as $|\Psi_{fin}\rangle = |s_i\rangle_{X_i} |\Phi\rangle_{\bar{X}_i}$ (\bar{X}_i is the complementary subsystem of X_i , and $s_i = \uparrow$ or \downarrow). From the \overline{G}_d representation viewpoint, it means that all the incoming vertices of w_i have the same color irrespective of the number of vertices. \square

By the above lemma, we can directly see that the $N = 5$ example (18) has a separable subsystem X_3 in $|\uparrow\rangle$, for w_3 has only blue incoming edges in its corresponding \overline{G}_d (26). Indeed, the explicit calculation in Eq. (25) shows that the subsystem X_3 is separable.

Note that even if all the vertices of a \overline{G}_d are in multiple cycles with both colors of incoming edges, the corresponding LQN can have a separable subsystem in a superposed state of $|\uparrow\rangle$ and $|\downarrow\rangle$. For

example,



generates a no-bunching state $T_{11}T_{22}T_{33}|\uparrow_1\uparrow_2\downarrow_3\rangle + T_{11}T_{23}T_{32}|\uparrow_1\downarrow_2\uparrow_3\rangle + T_{12}T_{21}T_{33}|\downarrow_1\uparrow_2\downarrow_3\rangle + T_{21}T_{32}T_{13}|\downarrow_1\downarrow_2\uparrow_3\rangle$. If we set $T_{1i} = T_{2i} = 1/\sqrt{3}$ and $T_{3i} = 1/\sqrt{2}$ for $i = 1, 2, 3$, the state becomes proportional to $(|\uparrow_1\rangle + |\downarrow_1\rangle)(|\uparrow_2\downarrow_3\rangle + |\downarrow_2\uparrow_3\rangle)$.

Second, the connectivity of a \overline{G}_d also discloses a separability condition of the LQN:

Lemma 2. *If a \overline{G}_d is disconnected as a k -partition of vertices $W_1|W_2|\dots|W_k$, then the no-bunching state of the LQN is k -separable under $\alpha_k = S_1|S_2|\dots|S_k$ where S_i is mapped to W_i ($i = 1, \dots, k$).*

Proof. For a set of vertices W_1 , we obtain PMs by taking edge exchanges only in W_1 . Then the corresponding state is a tensor product of a S_1 state and a \overline{S}_1 state. By taking the same kind of edge exchanges for all W_a ($\in \beta_k$) and sum the corresponding states, we obtain a state that is separable under $S_1|\overline{S}_1$. By repeating the same process for all W_i , we see that the no-bunching state is k -separable under α_k . \square

The \overline{G}_d (26) is also a good example for the application of the above lemma. Since (26) has two disconnected sets of vertices $\{w_1, w_3, w_4\}|\{w_2, w_5\}$, it must be biseparable under $(X_1, X_3, X_4)|(X_2, X_5)$. Indeed, Eq. (25) is rewritten in the tensor product form as

$$|\Psi_{fin}\rangle = \left[T_{11}T_{33}T_{44}|\downarrow_1\uparrow_4\rangle + T_{14}(T_{41}T_{33} + T_{43}T_{31})|\uparrow_1\downarrow_4\rangle \right] \otimes |\uparrow_3\rangle \left[T_{22}T_{55}|\downarrow_2\uparrow_5\rangle + T_{25}T_{52}|\uparrow_2\downarrow_5\rangle \right]. \quad (27)$$

Therefore, applying Lemma 1 and 2, we see that the $N = 5$ LQN (18) generates a 3-separable state under a 3-partition $(X_1, X_4)|(X_3)|(X_2, X_5)$.

Based on Lemma 1 and 2, we present the following theorem that provides necessary conditions for a \overline{G}_d with N vertices to be genuinely N -partite entangled.

Theorem 1. *If an LQN generates a genuinely entangled no-bunching state, then i) each vertex in the \overline{G}_d must have more than two incoming edges of different colors, and ii) all the vertices in it are strongly connected to each other (strong connection of w_i and w_j : we can move from w_i toward w_j and also from w_j toward w_i).*

Proof. Since Lemma 1 shows that the first condition is necessary, the remaining part of the proof is to show that the second condition is necessary. Using Lemma 2, all the vertices must be connected (i.e., have a path with each other) for an LQN to generate a genuinely entangled state. On the other hand, by Definition 1, all the edges in a \overline{G}_d must be in elementary cycles. Combining Lemma 2 and Definition 1, all the elementary cycles in the \overline{G}_d must be connected, which results in the strong connection between any pair of vertices. Therefore, the second condition is necessary for the generation of genuine entanglement. \square

The above theorem is useful not only for checking the separability of a given LQN, but also for designing LQNs. Indeed, when one tries to design an LQN for a specific genuinely entangled state, the connectivity and color distribution of the \overline{G}_d provide solid guidelines.

B. Designing LQNs for genuinely entangled states in the \overline{G}_d -representation

Now, we design \overline{G}_d s that generate fundamental N -partite genuinely entangled states, i.e., states in GHZ and W classes, and the Dicke state.

To achieve an arbitrary no-bunching state in an LQN that we expect, we can consider a ‘‘trial and error’’ method to construct a suitable \overline{G}_d that contains a given set of L PMs, which can be summarized as follows:

1. Among the L PMs, choose one PM to be mapped to a \overline{G}_d of N loops.
2. Map another PM to a \overline{G}_d with an elementary cycle so that there is no discrepant loop or edge with the first \overline{G}_d .
3. Repeat until we obtain L \overline{G}_d s.
4. Pile up all the \overline{G}_d s to obtain a \overline{G}_d that contains all the PMs.

It is guaranteed by construction that the final \overline{G}_d is mapped to an LQN that includes the L PMs.

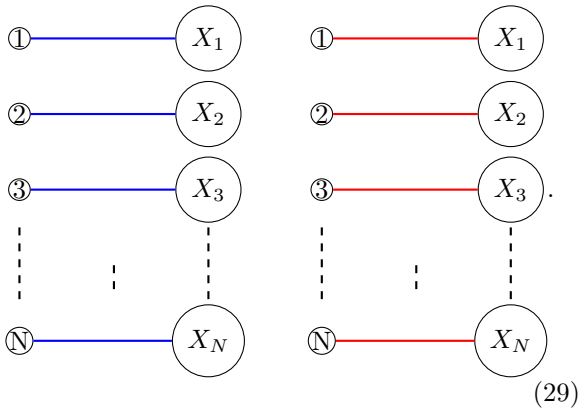
However, such constructed \overline{G}_d may also have unwanted PMs that are not in the L PMs. We call such a PM from the constructed \overline{G}_d a *superfluous PM*. While it is not clear whether an universal strategy exists for avoiding the superfluous PMs, we can find optimal strategies for some specific states, especially those in GHZ and W classes.

In the following, we use the insight of Section III A to construct LQNs for fundamental genuinely entangled states, i.e., those in the GHZ and W classes, and the Dicke state.

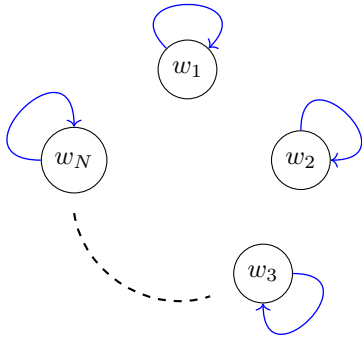
a. GHZ class generation. We start our discussion from the standard N -partite GHZ state,

$$|GHZ\rangle = \frac{1}{\sqrt{2}}(|\uparrow_1\uparrow_2\cdots\uparrow_N\rangle + |\downarrow_1\downarrow_2\cdots\downarrow_N\rangle). \quad (28)$$

There are two PMs for the state,

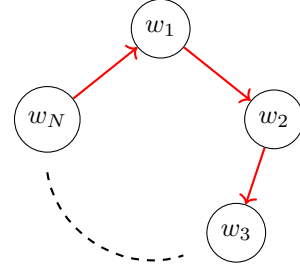


First, we choose the left one to be a \overline{G}_d of N loops,

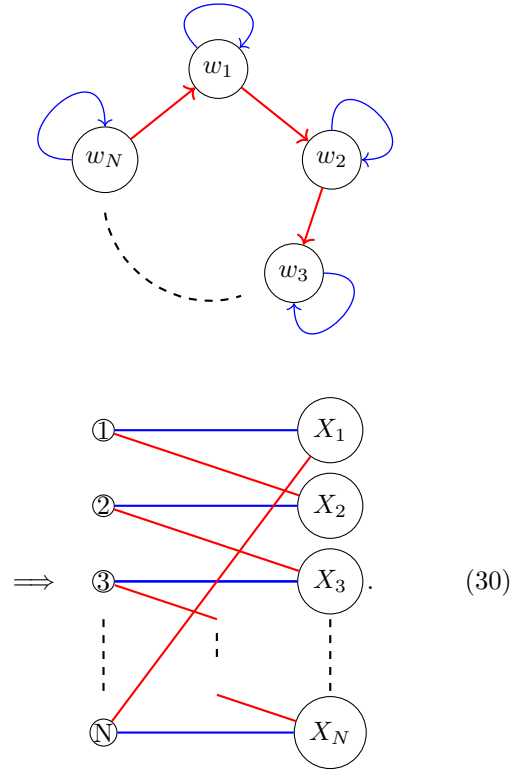


Then, any \overline{G}_d with a elementary cycle that involves all the vertices can be the second \overline{G}_d . One of such a

\overline{G}_d is



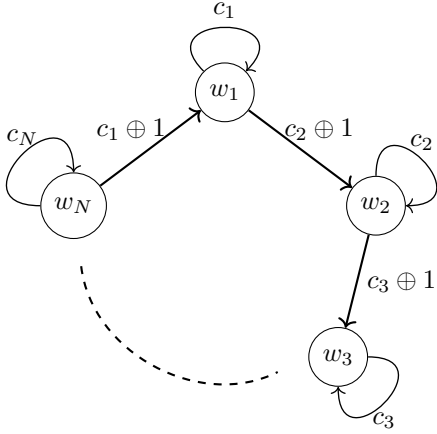
By piling up the two \overline{G}_d s, we obtain a \overline{G}_d that gives two PMs for the N -partite GHZ state,



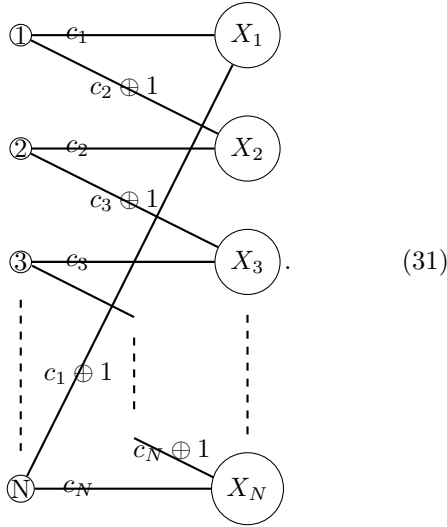
The above \overline{G}_d gives two PMs (29) without a superfluous PM.

Extending the above analysis, we can conceive PM diagrams for the GHZ basis of 2^N states, i.e., states that can transform with local operations to the standard GHZ state (28). Such PM diagrams has the same edge structure as (30) whose edge colors satisfy the necessary condition i) of Theorem 1. By setting the edge colors as c_j ($= B$ or R for $j = 1, \dots, N$), and denoting $c_j \oplus 1$ as the different color from c_j , we can see that the following \overline{G}_d constructs the GHZ

class:



The corresponding G_{bb} becomes



Indeed, the two PMs in (31) correspond to

$$|c_1, c_2, \dots, c_N\rangle + |c_1 \oplus 1, c_1 \oplus 1, \dots, c_N \oplus 1\rangle. \quad (32)$$

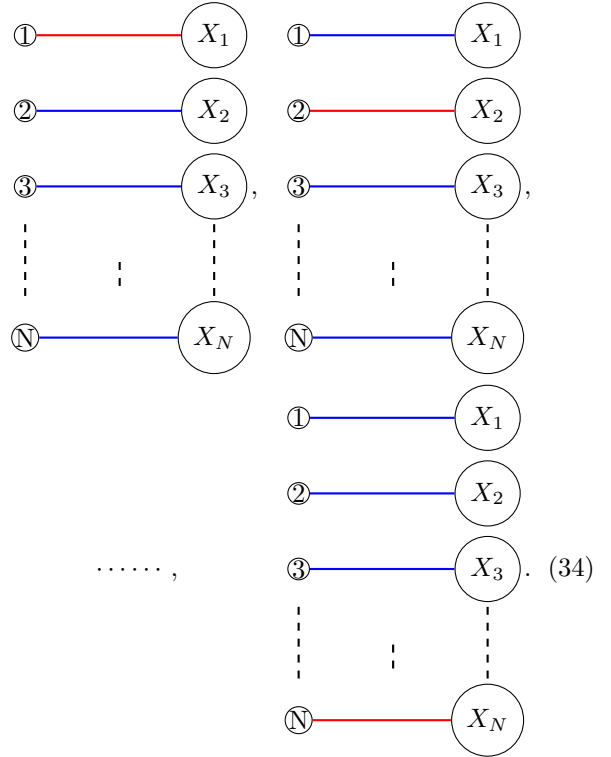
There are 2^N states of the above form, which construct the GHZ basis. The $N = 3$ GHZ basis example is explained in Appendix B.

b. W class generation. The standard W state is a permutation symmetric state with one subsystem in \downarrow , i.e.,

$$|W\rangle = \frac{1}{\sqrt{N}} (|\downarrow_1 \uparrow_2, \dots, \uparrow_N\rangle + |\uparrow_1 \downarrow_2 \dots \uparrow_N\rangle + \dots + |\uparrow_1 \uparrow_2 \dots \downarrow_N\rangle). \quad (33)$$

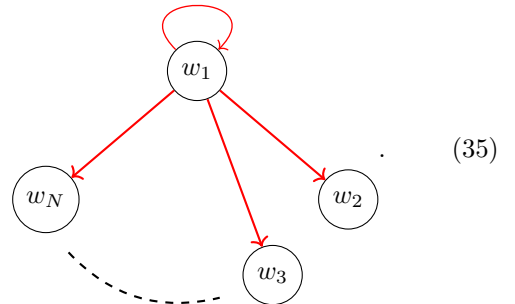
The expected G_{bb} has N PMs which contain one

red edge per PM, i.e.,



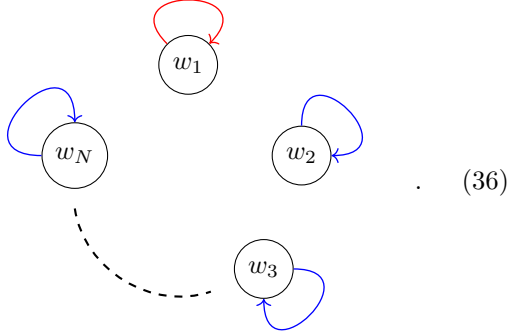
There are several options to draw LQNs for the above set of PMs. By analyzing the \bar{G}_d of such LQNs, we can find a crucial property for any LQN that generates an N -partite W state with no superfluous term, which we state in the language of \bar{G}_d as the following theorem:

Theorem 2. *Suppose that a \bar{G}_d is optimal for the N -partite W state, i.e., in the \bar{G}_d , all the PMs for the N -partite W-state appear once with no superfluous PM. Then, the \bar{G}_d must have N red edges that leave the same vertex, i.e., the N red edges must distribute without loss of generality as*



Proof. First, we can map the first PM of (34) to N

loops,



Since the edge $(1, X_1)$ is red in only one PM, all the elementary cycles must pass w_1 to exchange the red loop of w_1 with other incoming blue edges. In addition, the optimal \overline{G}_d for the W state has $(N-1)$ -elementary cycles and each elementary cycle must have a different red edge from those in the other elementary cycles.

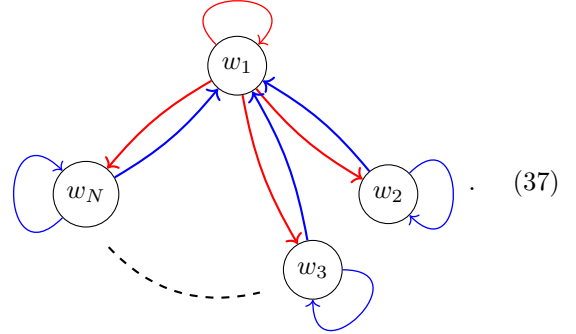
Using the above restrictions, we first show that if $(w_1 \rightarrow w_j)$ exists for some j ($2 \leq j \leq N$), then it must be red, i.e., $(w_1 \xrightarrow{R} w_j)$. Suppose $(w_1 \xrightarrow{B} w_j)$. Then, since w_j must have one red incoming edge, there exists an edge $(w_l \xrightarrow{R} w_j)$ where l is neither 1 nor j . On the other hand, w_l also must have one red incoming edge. From the fact that w_1 is in all elementary cycles, we see that there exists at least one elementary cycle that includes the two red edges. This contradicts with the restriction that each elementary cycle must have only one red edge. Therefore, $(w_1 \rightarrow w_j)$ must be red.

Now, we show that $(w_1 \rightarrow w_j)$ exists for all j ($= 2, \dots, N$). Suppose that an edge $(w_1 \rightarrow w_k)$ ($2 \leq k \leq N$) is absent. Then, considering there must be $(N-1)$ -elementary cycles that pass w_1 , an edge $(w_1 \rightarrow w_l)$ ($2 \leq l \leq N$) must be included in more than one elementary cycle. Since no two elementary cycles can have the same red edge, $(w_1 \rightarrow w_k)$ must be blue, i.e., $(w_1 \xrightarrow{B} w_k)$, which is not possible as we have shown. Therefore, the N red edges must distribute as (35). \square

According to the above theorem, we see that an LQN that carries a W state must have one identical particle that can be observed at all detectors as \downarrow , while all other particles are observed as \uparrow .

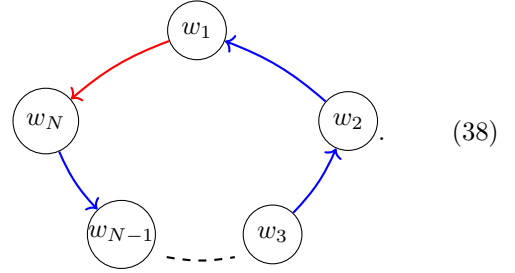
Using Theorems 1 and 2, we suggest two ways to design LQNs for the W state. The first one consists only of $(w_1 \xrightarrow{R} w_a \xrightarrow{B} w_1)$ where $a = 2, \dots, N$. By piling up such $(N-1)$ -elementary cycles and (36),

we obtain a \overline{G}_d ,

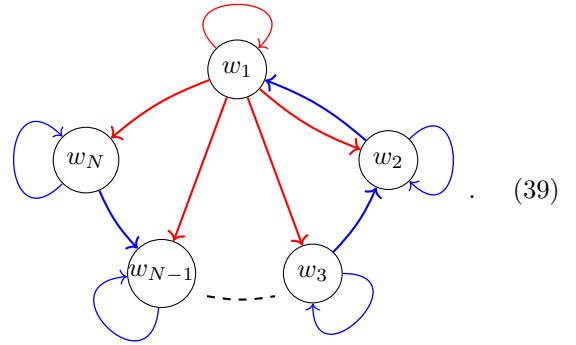


We see that each elementary cycle includes one red edge, which gives a PM that composes the N -partite W state.

Another \overline{G}_d can contain an elementary cycle of N vertices $(w_1 \xrightarrow{R} w_N \xrightarrow{B} \dots \xrightarrow{B} w_2 \xrightarrow{B} w_1)$,



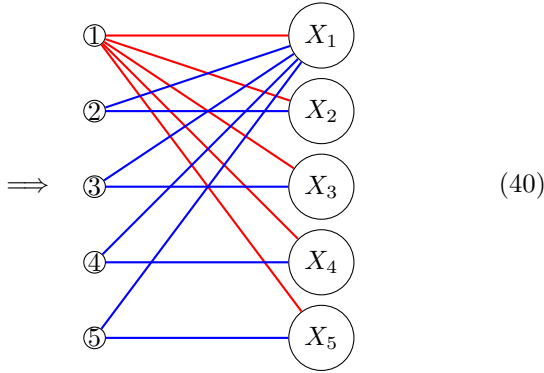
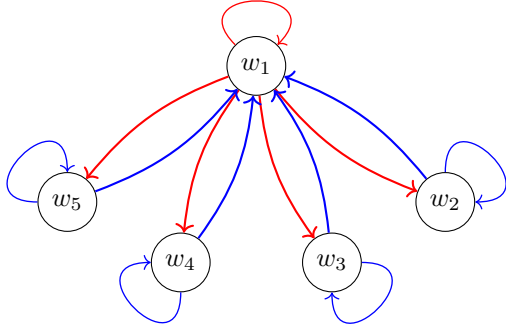
By piling up (35) with the above, we have



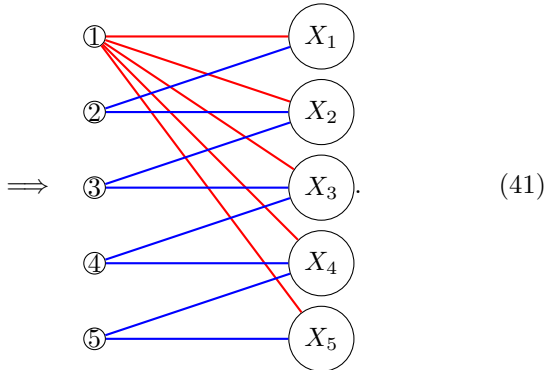
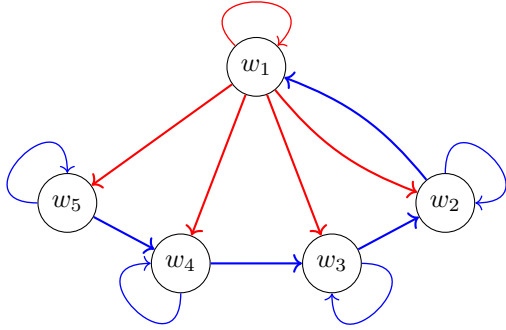
The $(N-1)$ -elementary cycles are of the form $(w_1 \xrightarrow{R} w_j \xrightarrow{B} w_{j-1} \xrightarrow{B} \dots \xrightarrow{B} w_2 \xrightarrow{B} w_1)$ where $j = 2, \dots, N$, which also gives PMs that construct the N -partite W state. It is direct to see that (37) and (39) satisfy the necessary conditions of Theorems 1 and 2.

For example, when $N = 5$, (37) and its corre-

sponding G_{bb} are given by



And (39) and its corresponding G_{bb} for $N = 5$ are given by

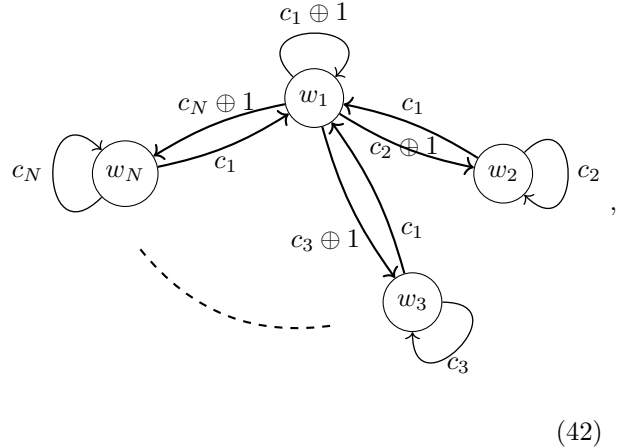


It is worth mentioning other forms of LQNs that

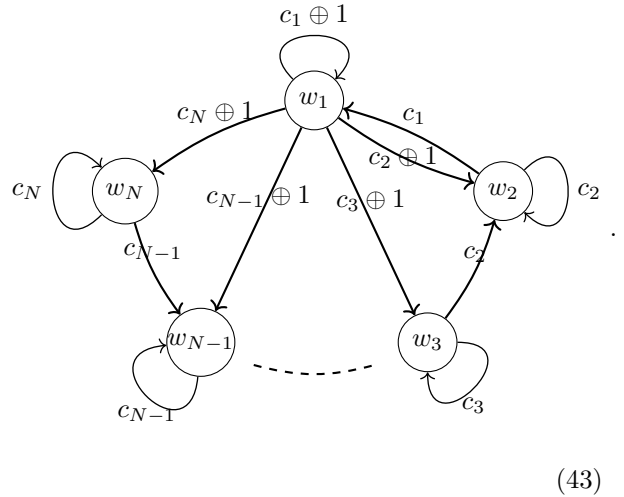
can generate the W state. The \overline{G}_d of the tritter LQN (Eq. (16)) generates a W state by including the same PM twice. We can also generate a W state using an ancilla as suggested in Refs. [11–13].

Similar to the GHZ case, we can consider PM diagrams that build the W basis of 2^N states. One group of the PM diagrams has the same edge structure as (37), and the other has the same structure as (39). In each group, the edge colors satisfy the necessary condition i) of Theorem 1.

The first group is of the form



and the second group



The above PM diagrams has N PMs that correspond to the states of the W class. The $N = 3$ W basis example is explained in Appendix B.

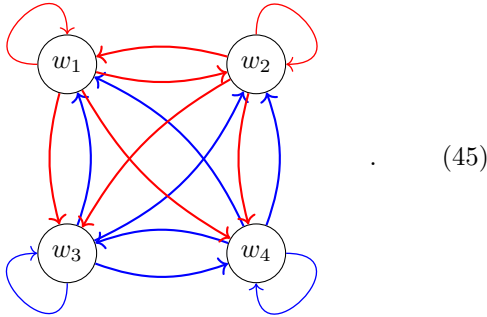
c. Dicke state generation The Dicke state $|D_k^N\rangle$ ($1 \leq k \leq N - 1$) is a permutation symmetric state with k subsystems in \downarrow . Here, we provide a \overline{G}_d for the $k = 2$ Dicke state. A \overline{G}_d for an arbitrary k case can be conceived by induction from the W state case (37) and the D_2^N case that we will discuss here.

The $k = 2$ Dicke state can be expressed as

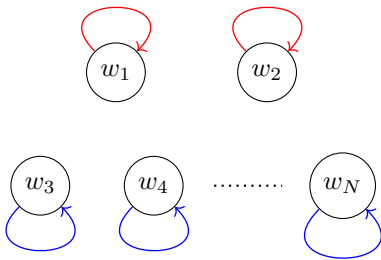
$$|D_2^N\rangle = \frac{1}{\sqrt{\binom{N}{2}}} \sum_p |\downarrow_{p_1} \downarrow_{p_2}, \uparrow_{p_3}, \dots, \uparrow_{p_N}\rangle \quad (44)$$

where the summation is over all the permutations of $(1, 2, \dots, N)$ that gives different states. This is represented as $\frac{N(N-1)}{2}$ PMs that consist of $(N-2)$ blue edges and 2 red edges.

One can easily consider an LQN for $|D_2^N\rangle$ in analogy to the tritter LQN for the W state, i.e., sending $(N-2)$ -particles in \uparrow and 2 particles in \downarrow to N detectors through a balanced unitary operator. For example, $|D_2^4\rangle$ can be generated by the following LQN:

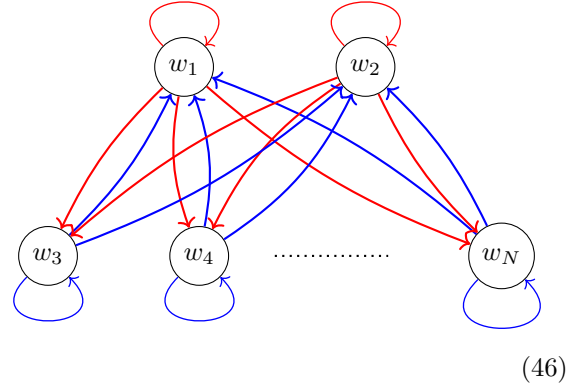


On the other hand, we can also generate $|D_2^N\rangle$ with an LQN of less edges in analogy to (37) for the W state. We can conceive a \bar{G}_d for $|D_2^N\rangle$ based on the following N loops

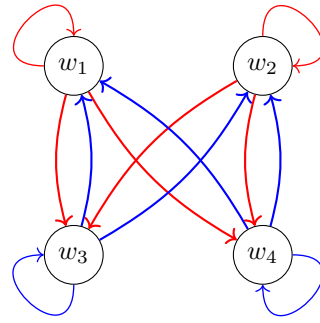


and $2(N-2)$ -cycles $(w_j \xrightarrow{R} w_k \xrightarrow{B} w_j)$ where $j = 1, 2$

and $k = 3, 4, \dots, N$:



Examining all elementary cycles, we see that the above LQN gives all PMs that construct $|D_2^N\rangle$ state (see Appendix C for the final no-bunching state of the above \bar{G}_d). However, unlike the LQNs for GHZ and W state we have proposed, not all PMs from (46) appear once. Indeed, by expressing a state with i th and j th subsystems in \downarrow as $|\bar{n}_{ij}\rangle$, there are four states of $|\bar{n}_{kl}\rangle$ for $k \neq 1, 2$ and $l \neq 1, 2$. For the simplest $N = 4$ example, (46) is drawn as



Its corresponding G_{bb} and LQN are given in Fig. 1. The postselected no-bunching state is given, with the T_{ij} as the amplitude from i to X_j , by

$$\begin{aligned} & T_{11}T_{22}T_{33}T_{44} |\downarrow_1 \downarrow_2 \uparrow_3 \uparrow_4\rangle \\ & + T_{11}T_{44}T_{32}T_{23} |\downarrow_1 \uparrow_2 \downarrow_3 \uparrow_4\rangle \\ & + T_{11}T_{33}T_{42}T_{24} |\downarrow_1 \uparrow_2 \uparrow_3 \downarrow_4\rangle \\ & + T_{22}T_{44}T_{31}T_{13} |\uparrow_1 \downarrow_2 \downarrow_3 \uparrow_4\rangle \\ & + T_{14}T_{22}T_{33}T_{41} |\uparrow_1 \downarrow_2 \uparrow_3 \downarrow_4\rangle \\ & + (T_{13}T_{31}T_{24}T_{42} + T_{23}T_{32}T_{14}T_{41} \\ & + T_{13}T_{32}T_{24}T_{41} + T_{14}T_{42}T_{23}T_{31}) |\uparrow_1 \uparrow_2 \downarrow_3 \downarrow_4\rangle. \end{aligned} \quad (47)$$

As we have mentioned, $|\uparrow_1 \uparrow_2 \downarrow_3 \downarrow_4\rangle = |\bar{n}_{34}\rangle$ appears four times in the LQN. The amplitude of the

state can be factorized as $(T_{13}T_{24}+T_{23}T_{14})(T_{31}T_{42}+T_{32}T_{41})|\uparrow_1\uparrow_2\downarrow_3\downarrow_4\rangle$.

However, we can still achieve the standard $|D_2^4\rangle$ by properly fixing the amplitude phases. Indeed, it can be easily checked that the following imposition of amplitudes presents the standard $|D_2^4\rangle$:

$$\begin{aligned} T_{11} = T_{22} = T_{33} = T_{44} &= \frac{1}{\sqrt{3}}, \\ T_{13} = \frac{e^{\frac{i\pi}{6}}}{\sqrt{3}} = T_{31}^*, \quad T_{14} &= \frac{e^{-\frac{i\pi}{6}}}{\sqrt{3}} = T_{41}^*, \\ T_{23} = \frac{e^{-\frac{i\pi}{6}}}{\sqrt{3}} = T_{32}^*, \quad T_{24} &= \frac{e^{\frac{i\pi}{6}}}{\sqrt{3}} = T_{42}^*. \end{aligned} \quad (48)$$

We discuss further on the $N = 5$ case in Appendix C.

IV. CONCLUSIONS

By introducing a strict mapping relation of LQNs into graphs, we have shown that the entanglement generation in LQN can be efficiently analyzed with graph theory techniques. Other than the LQNs for genuine entanglement that we have explained here, we can find numerous LQNs for multipartite genuinely entangled states that have intriguing physical properties and can be verified experimentally [35].

We can apply the graph picture of LQNs to more general cases. For example, the original boson sampling setup with $N \ll M$ also postselects no-bunching states [15]. Thus, we expect that our computation technique for no-bunching states would be useful for understanding the quantum complexity of boson sampling. Moreover, we can also consider a mapping relation of LQNs and graphs when the final internal state r_j^a of each particle can be a superposition of \uparrow and \downarrow . Optics realizes this type of transformations with *partially polarizing beamsplitters* (PPBS), which correspond to the partial collapse measurements that can suppress decoherence effects [36] and handily implement CNOT gates [37–39]. While our current work have mapped LQNs into G_{bb} s that are simple (neither loops nor multiple edges), the generalized mapping would need multi-graphs (permitting multiple edges between vertices).

ACKNOWLEDGEMENTS

We appreciate Dr. Hyang-Tag Lim, Dr. Young-Wook Cho, and Dongwha Lee for helpful discussion. S.C. is also grateful to Prof. Jung-Hoon Chun for

his support during the research. This work is supported by the National Research Foundation of Korea (NRF, NRF-2019R1I1A1A01059964 and NRF-2019M3E4A1079777).

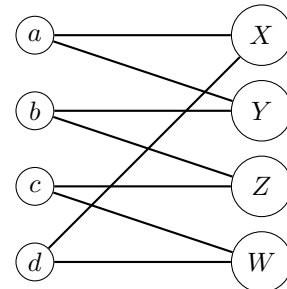
Appendix A: Graph theory glossary

a. Graph— A **graph** $G = (V, E)$ is a collection of vertices V and edges E that connects the elements in V . Each edge can have a **color** and a **weight**. An edge weight is a numerical value associated to the edge. In this paper, it is considered a complex number.

b. Undirected and directed graphs— Edges in a graph can have direction or not. An **undirected graph** is made of undirected edges, and a **directed graph** (or digraph, G_d) of directed edges. For an undirected graph $G = (V, E)$ with $V = \{v_1, v_2, \dots, v_N\}$, an edge ($\in E$) that connects v_i and v_j is denoted as (v_i, v_j) . For a $G_d = (W, F)$ with $W = \{w_1, w_2, \dots, w_N\}$, an edge ($\in F$) that connects w_i and w_j is denoted as $(w_i \rightarrow w_j)$.

For G_d , two vertices w_i and w_j are **strongly connected** if we can move from w_i toward w_j and from w_j toward w_i by following the edge directions. If a path in a G_d is of the form $(w_i \rightarrow \dots \rightarrow w_i)$ and w_i is the only repeated vertex in the path, it is called an **elementary cycle**.

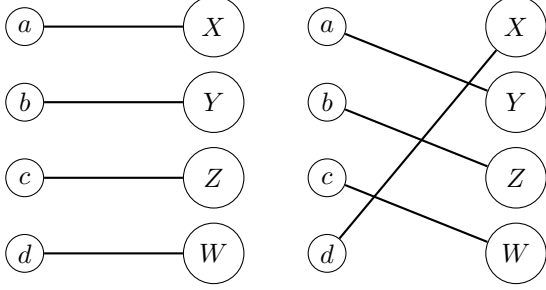
c. Bipartite graph and perfect matching— A **bipartite graph** (or bigraph, $G_b = (U \cup V, E)$) has two disjoint sets of vertices, U and V , such that every edge connects a vertex in U to another vertex in V . A bigraph is **balanced** if the number of vertices in U is equal to the number of vertices in V , i.e., $|U| = |V|$. Balanced bigraphs are denoted as G_{bb} . For example, with $U = \{a, b, c, d\}$ and $V = \{X, Y, Z, W\}$, a graph



is a G_{bb} .

A G_{bb} can have **perfect matchings** (PMs). A PM is an independent set of edges in which every vertex of U is connected to exactly one edge of V . If an edge ($\in E$) is in a PM, it is **maximally match-**

able. There are two PMs of the above G_{bb} :



Since no edge is out of a PM, all edges of the G_{bb} are maximally matchable.

d. *Adjacency matrix*.— The adjacency matrix of a graph is the matrix A with

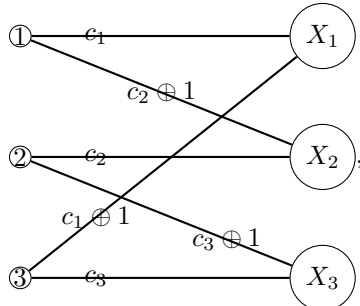
$$\begin{cases} A_{ij} = 0 & \text{if } v_i \text{ is not adjacent to } v_j \\ A_{ij} \neq 0 & \text{if } v_i \text{ is adjacent to } v_j \end{cases}$$

Since if v_i is adjacent to v_j then v_j is adjacent to v_i and vice versa in an undirected graph, the adjacency matrix of the graph is symmetric. Conversely, if an adjacency matrix is symmetric, then we can regard its corresponding graph as undirected.

By inserting the edge weights into the nonzero A_{ij} , we obtain the weighted adjacency matrix. By inserting the edge colors instead, we obtain the colored adjacency matrix.

Appendix B: $N = 3$ GHZ and W basis

a. $N = 3$ GHZ basis.— For the $N = 3$ case, the G_{bb} -representation of (31) becomes

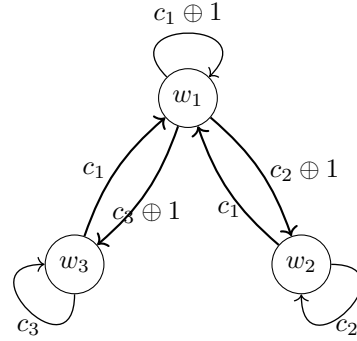


which has two PMs

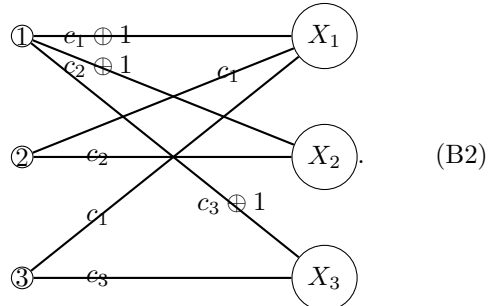
$$= T_{11}T_{22}T_{33}|c_1, c_2, c_3\rangle + T_{12}T_{23}T_{31}|c_1 \oplus 1, c_2 \oplus 2, c_3 \oplus 3\rangle. \quad (\text{B1})$$

By varying (c_1, c_2, c_3) , we obtain the eight states that construct a GHZ basis (see, e.g., [40]).

b. $N = 3$ W basis.— From (42), we have



whose G_{bb} is

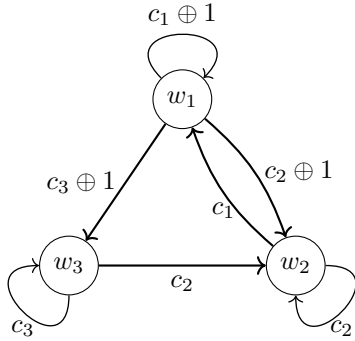


There are three PMs,

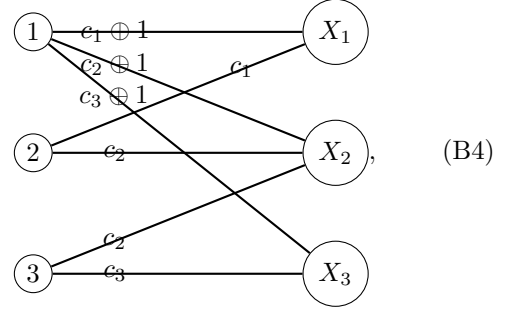
$$\begin{aligned}
 & \textcircled{1} \xrightarrow{e_1 \oplus 1} X_1 & \textcircled{1} \xrightarrow{c_2 \oplus 1} X_1 \\
 & \textcircled{2} \xrightarrow{e_2} X_2 & \textcircled{2} \xrightarrow{c_1} X_2 \\
 & \textcircled{3} \xrightarrow{e_3} X_3 & \textcircled{3} \xrightarrow{e_3} X_3 \\
 & \textcircled{1} \xrightarrow{c_3 \oplus 1} X_1 & \\
 & \textcircled{2} \xrightarrow{e_2} X_2 & \\
 & \textcircled{3} \xrightarrow{c_1} X_3 & \\
 & = T_{11}T_{22}T_{33}|c_1 \oplus 1, c_2, c_3\rangle & \\
 & \quad + T_{21}T_{12}T_{33}|c_1, c_2 \oplus 1, c_3\rangle & \\
 & \quad + T_{31}T_{13}T_{22}|c_1, c_2, c_3 \oplus 1\rangle, & \tag{B3}
 \end{aligned}$$

which construct the W basis [40].

From (43), we have



whose G_{bb} is



which has three PMs,

$$\begin{aligned}
 & \textcircled{1} \xrightarrow{e_1 \oplus 1} X_1 & \textcircled{1} \xrightarrow{c_2 \oplus 1} X_1 \\
 & \textcircled{2} \xrightarrow{e_2} X_2 & \textcircled{2} \xrightarrow{c_1} X_2 \\
 & \textcircled{3} \xrightarrow{e_3} X_3 & \textcircled{3} \xrightarrow{e_3} X_3 \\
 & \textcircled{1} \xrightarrow{c_1} X_1 & \\
 & \textcircled{2} \xrightarrow{c_3 \oplus 1} X_2 & \\
 & \textcircled{3} \xrightarrow{c_2} X_3 & \\
 & = T_{11}T_{22}T_{33}|c_1 \oplus 1, c_2, c_3\rangle & \\
 & \quad + T_{21}T_{12}T_{33}|c_1, c_2 \oplus 1, c_3\rangle & \\
 & \quad + T_{21}T_{32}T_{13}|c_1, c_2, c_3 \oplus 1\rangle. & \tag{B5}
 \end{aligned}$$

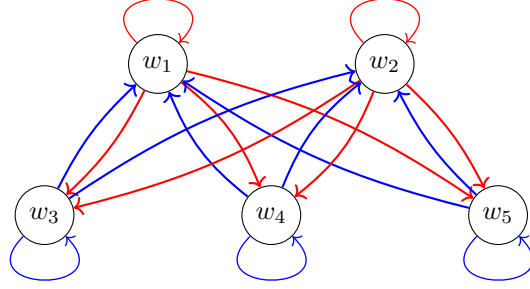
We see that the final result is equal to (B3).

Appendix C: D_2^N state generation

The postselected no-bunching state from (46) is given by

$$\begin{aligned}
 & \left(\prod_{i=1}^N T_{ii} \right) |\vec{n}_{12}\rangle + \sum_{j=3}^N \left(\prod_{i \neq 2, j}^N T_{ii} \right) T_{j2}T_{2j} |\vec{n}_{1j}\rangle + \sum_{j=3}^N \left(\prod_{i \neq j}^N T_{ii} \right) T_{j1}T_{1j} |\vec{n}_{2j}\rangle \\
 & + \sum_{3 \leq j < k \leq N} \left(\prod_{i \neq j, k}^N T_{ii} \right) (T_{1j}T_{2k} + T_{2j}T_{1k})(T_{j2}T_{k1} + T_{j1}T_{k2}) |\vec{n}_{jk}\rangle, & \tag{C1}
 \end{aligned}$$

where $|\vec{n}_{ij}\rangle$ denotes a state with i th and j th subsystems in \downarrow . One can see that there are four states of $|\vec{n}_{kl}\rangle$ for $k \neq 1, 2$ and $l \neq 1, 2$. We can check whether the standard D_2^N state from the above state can be obtained by controlling the amplitudes. For the $N = 5$ case, the \overline{G}_d is drawn as



Then, the final no-bunching state is given by

$$\begin{aligned}
& T_{11}T_{22}T_{33}T_{44}T_{55}|\downarrow_1\downarrow_2\uparrow_3\uparrow_4\uparrow_5\rangle + T_{11}T_{44}T_{55}T_{32}T_{23}|\downarrow_1\uparrow_2\downarrow_3\uparrow_4\uparrow_5\rangle + T_{11}T_{33}T_{55}T_{42}T_{24}|\downarrow_1\uparrow_2\uparrow_3\downarrow_4\uparrow_5\rangle \\
& + T_{11}T_{33}T_{44}T_{52}T_{25}|\downarrow_1\uparrow_2\uparrow_3\uparrow_4\downarrow_5\rangle + T_{22}T_{44}T_{55}T_{31}T_{13}|\uparrow_1\downarrow_2\downarrow_3\uparrow_4\uparrow_5\rangle + T_{22}T_{33}T_{55}T_{14}T_{41}|\uparrow_1\downarrow_2\uparrow_3\downarrow_4\uparrow_5\rangle \\
& + T_{22}T_{33}T_{44}T_{15}T_{51}|\uparrow_1\downarrow_2\uparrow_3\uparrow_4\downarrow_5\rangle + T_{55}(T_{13}T_{24} + T_{23}T_{14})(T_{32}T_{41} + T_{31}T_{42})|\uparrow_1\uparrow_2\downarrow_3\downarrow_4\uparrow_5\rangle \\
& + T_{44}(T_{13}T_{25} + T_{23}T_{15})(T_{32}T_{51} + T_{31}T_{52})|\uparrow_1\uparrow_2\downarrow_3\uparrow_4\downarrow_5\rangle \\
& + T_{33}(T_{14}T_{25} + T_{24}T_{15})(T_{42}T_{51} + T_{41}T_{52})|\uparrow_1\uparrow_2\uparrow_3\downarrow_4\downarrow_5\rangle.
\end{aligned} \tag{C2}$$

We obtain the standard D_2^5 state by setting the transformation amplitudes as

$$\begin{aligned}
T_{11} = T_{22} &= \frac{1}{\sqrt{4}}, & T_{33} = T_{44} = T_{55} &= \frac{1}{\sqrt{3}}, \\
T_{13} &= \frac{1}{\sqrt{4}}, & T_{14} &= \frac{e^{-\frac{i\pi}{3}}}{\sqrt{4}}, & T_{15} &= \frac{e^{-\frac{2i\pi}{3}}}{\sqrt{4}}, & (T_{j1} = T_{1j}^*) \\
T_{23} &= \frac{e^{-\frac{i\pi}{3}}}{\sqrt{4}}, & T_{24} &= \frac{1}{\sqrt{4}}, & T_{25} &= \frac{e^{\frac{i\pi}{3}}}{\sqrt{4}}. & (T_{j2} = T_{2j}^*)
\end{aligned} \tag{C3}$$

-
- [1] R. Horodecki, P. Horodecki, M. Horodecki, and K. Horodecki, Quantum entanglement, *Reviews of modern physics* **81**, 865 (2009).
 - [2] C.-K. Hong, Z.-Y. Ou, and L. Mandel, Measurement of subpicosecond time intervals between two photons by interference, *Physical Review Letters* **59**, 2044 (1987).
 - [3] M. C. Tichy, F. de Melo, M. Kuš, F. Mintert, and A. Buchleitner, Entanglement of identical particles and the detection process, *Fortschritte der Physik* **61**, 225 (2013).
 - [4] N. Killoran, M. Cramer, and M. B. Plenio, Extracting entanglement from identical particles, *Physical Review Letters* **112**, 150501 (2014).
 - [5] M. Krenn, A. Hochrainer, M. Lahiri, and A. Zeilinger, Entanglement by path identity, *Physical Review Letters* **118**, 080401 (2017).
 - [6] N. Paunkovic, *The role of indistinguishability of identical particles in quantum information processing*, Ph.D. thesis, University of Oxford (2004).
 - [7] R. L. Franco and G. Compagno, Indistinguishability of elementary systems as a resource for quantum information processing, *Physical Review Letters* **120**, 240403 (2018).
 - [8] S. Chin and J. Huh, Entanglement of identical particles and coherence in the first quantization language, *Physical Review A* **99**, 052345 (2019).
 - [9] F. Nosrati, A. Castellini, G. Compagno, and R. L. Franco, Robust entanglement preparation against noise by controlling spatial indistinguishability, *npj Quantum Information* **6**, 1 (2020).
 - [10] M. R. Barros, S. Chin, T. Pramanik, H.-T. Lim, Y.-W. Cho, J. Huh, and Y.-S. Kim, Entangling bosons through particle indistinguishability and spatial overlap, *Optics Express* **28**, 38083 (2020).
 - [11] B. Bellomo, R. L. Franco, and G. Compagno, N identical particles and one particle to entangle them all, *Physical Review A* **96**, 022319 (2017).
 - [12] Y.-S. Kim, Y.-W. Cho, H.-T. Lim, and S.-W. Han, Efficient linear optical generation of a multipartite

- w state via a quantum eraser, *Physical Review A* **101**, 022337 (2020).
- [13] P. Blasiak and M. Markiewicz, Entangling three qubits without ever touching, *Scientific Reports* **9** (2019).
- [14] J.-D. Urbina, J. Kuipers, S. Matsumoto, Q. Hummel, and K. Richter, Multiparticle correlations in mesoscopic scattering: Boson sampling, birthday paradox, and hong-ou-mandel profiles, *Physical Review Letters* **116**, 100401 (2016).
- [15] S. Aaronson and A. Arkhipov, The computational complexity of linear optics, in *Proceedings of the forty-third annual ACM symposium on Theory of computing* (2011) pp. 333–342.
- [16] H.-S. Zhong, H. Wang, Y.-H. Deng, M.-C. Chen, L.-C. Peng, Y.-H. Luo, J. Qin, D. Wu, X. Ding, Y. Hu, *et al.*, Quantum computational advantage using photons, *Science* **370**, 1460 (2020).
- [17] P. Blasiak, E. Borsuk, and M. Markiewicz, On safe post-selection for bell nonlocality: Causal diagram approach, arXiv preprint arXiv:2012.07285 (2020).
- [18] W. Dür, H. Aschauer, and H.-J. Briegel, Multiparticle entanglement purification for graph states, *Physical Review Letters* **91**, 107903 (2003).
- [19] M. Hein, J. Eisert, and H. J. Briegel, Multiparty entanglement in graph states, *Physical Review A* **69**, 062311 (2004).
- [20] M. Van den Nest, J. Dehaene, and B. De Moor, Local unitary versus local clifford equivalence of stabilizer states, *Physical Review A* **71**, 062323 (2005).
- [21] M. Hein, W. Dür, J. Eisert, R. Raussendorf, M. Nest, and H.-J. Briegel, Entanglement in graph states and its applications, arXiv preprint quant-ph/0602096 (2006).
- [22] M. Krenn, X. Gu, and A. Zeilinger, Quantum experiments and graphs: Multiparty states as coherent superpositions of perfect matchings, *Physical Review Letters* **119**, 240403 (2017).
- [23] X. Gu, M. Erhard, A. Zeilinger, and M. Krenn, Quantum experiments and graphs ii: Quantum interference, computation, and state generation, *Proceedings of the National Academy of Sciences* **116**, 4147 (2019).
- [24] X. Gu, L. Chen, A. Zeilinger, and M. Krenn, Quantum experiments and graphs. iii. high-dimensional and multiparticle entanglement, *Physical Review A* **99**, 032338 (2019).
- [25] X. Gu, L. Chen, and M. Krenn, Quantum experiments and hypergraphs: Multiphoton sources for quantum interference, quantum computation, and quantum entanglement, *Physical Review A* **101**, 033816 (2020).
- [26] K. Brádler, P.-L. Dallaire-Demers, P. Reberntrost, D. Su, and C. Weedbrook, Gaussian boson sampling for perfect matchings of arbitrary graphs, *Physical Review A* **98**, 032310 (2018).
- [27] J. M. Arrazola and T. R. Bromley, Using gaussian boson sampling to find dense subgraphs, *Physical Review Letters* **121**, 030503 (2018).
- [28] K. Bradler, S. Friedland, J. Izaac, N. Killoran, and D. Su, Graph isomorphism and gaussian boson sampling, arXiv preprint arXiv:1810.10644 (2018).
- [29] In the most general sense, we can consider a transformation T so that r_j^a becomes a superposition of \uparrow and \downarrow , which we put off to our future research. Such an LQN includes, e.g., partially polarizing beam splitter (PPBS) in linear optics [36–39].
- [30] R. A. Brualdi, F. Harary, and Z. Miller, Bigraphs versus digraphs via matrices, *Journal of Graph Theory* **4**, 51 (1980).
- [31] K. Fukuda and T. Matsui, Finding all the perfect matchings in bipartite graphs, *Applied Mathematics Letters* **7**, 15 (1994).
- [32] T. Tassa, Finding all maximally-matchable edges in a bipartite graph, *Theoretical Computer Science* **423**, 50 (2012).
- [33] M. Seevinck and J. Uffink, Partial separability and entanglement criteria for multiqubit quantum states, *Physical Review A* **78**, 032101 (2008).
- [34] S. Szalay and Z. Kökényesi, Partial separability revisited: Necessary and sufficient criteria, *Physical Review A* **86**, 032341 (2012).
- [35] S. Chin, D. Lee, and Y.-S. Kim, Multipartite entangled states of linear quantum networks: a graph theoretic approach, in preparation.
- [36] Y.-S. Kim, J.-C. Lee, O. Kwon, and Y.-H. Kim, Protecting entanglement from decoherence using weak measurement and quantum measurement reversal, *Nature Physics* **8**, 117 (2012).
- [37] N. K. Langford, T. Weinhold, R. Prevedel, K. Resch, A. Gilchrist, J. O’Brien, G. Pryde, and A. White, Demonstration of a simple entangling optical gate and its use in bell-state analysis, *Physical Review Letters* **95**, 210504 (2005).
- [38] N. Kiesel, C. Schmid, U. Weber, R. Ursin, and H. Weinfurter, Linear optics controlled-phase gate made simple, *Physical Review Letters* **95**, 210505 (2005).
- [39] R. Okamoto, H. F. Hofmann, S. Takeuchi, and K. Sasaki, Demonstration of an optical quantum controlled-not gate without path interference, *Physical Review Letters* **95**, 210506 (2005).
- [40] M. M Cunha, A. Fonseca, and E. O Silva, Tripartite entanglement: Foundations and applications, *Universe* **5**, 209 (2019).